This is a preprint, the final version is subject to change, of the American Mineralogist (MSA)
Cite as Authors (Year) Title. American Mineralogist, in press.
(DOI will not work until issue is live.) DOI: http://dx.doi.org/10.2138/am.2013.4212

Revision 1

Acceleration and inhibition effects of phosphate on phase transformation of amorphous calcium carbonate into vaterite

Yuki Sugiura[1,3*], Kazuo Onuma[2*], Yuki Kimura[3,4], Katsuo Tsukamoto[3] and Atsushi Yamazaki[1]

1: *Department of Environmental and Resources Engineering, School of Creative Science and Technology, Waseda University, 3-4-1 Okubo, Shinjuku-ku, Tokyo 169-8555, Japan*

2*: National Institute of Advanced Industrial Science and Technology, Central 6, Higashi 1-1-1, Tsukuba, Ibaraki 305-8566, Japan*

3*: Earth and Planetary Science, Department of Science, Tohoku University, Aoba-ku, Aramaki, Sendai, Miyagi 980-0845, Japan*

4*: The Center of Interdisciplinary Research, Tohoku University, Aoba-ku, Aramaki, Sendai, Miyagi 980-0845, Japan*

*Corresponding authors: Kazuo Onuma and Yuki Sugiura

Email: k.onuma@aist.go.jp (K.O), arch.quartz@gmail.com (Y.S.)

Abstract

Phase transformation of amorphous calcium carbonate (ACC) into vaterite and its subsequent stability was investigated at a constant pH (~8.2), ionic strength, and temperature that simulated the biological environment. Solutions containing the same concentrations of $CaCl_2$, Na_2CO_3, and tris(hydroxymethyl)aminomethane buffer and various concentrations of PO_4 (0-62.5 μM) were prepared, and precipitates in the solutions were sampled at a constant interval to observe the morphology and type of calcium carbonate polymorphs that appeared. The change in the Ca-ion concentration over time, which served as a guide for phase transformation of ACC into crystalline phases, was measured in relation to the PO_4 concentration. The starting time of phase transformation was at the minimum point when the concentration was ~2-3 μM. Vaterite spherulites consisting of needle-like crystals (0.5-2 μm in length) formed only in this PO_4 range and survived the experimental procedure (~2.5 h). In contrast, the starting time of phase transformation increased exponentially with the PO_4 concentration when it was higher than 5 μM. The vaterite spherulites and calcite crystals co-precipitated, and both polymorphs grew over time. The PO_4 was shown to be an accelerator for phase transformation from ACC into vaterite at low concentrations (Ca/PO_4 molar ratio less than 3000) and an inhibitor for transformation at high concentrations. We investigated the kinetics of vaterite formation in the presence of PO_4 and derived an advanced concept for cluster-based phase transformation. This investigation showed that the appearance and stability of calcium carbonate polymorphs is easily controlled by adjusting the PO_4 concentration.

1. Introduction

Calcium carbonates are the main component of the hard tissue in non-vertebrates and are found, for example, in shells and coral reefs. They have at least six polymorphs, including calcite, vaterite, aragonite, amorphous calcium carbonate (ACC), and two hydrous phases. They form as a result of metabolism in biological organisms, a process known as "biomineralization." Biomineralization occurs under normal pressure and temperature in an aqueous solution with neutral to weak basic pH, indicating that it is a gentle crystallization process (Mann 2001, Sunagawa 2005, Weiner et al. 2003). The final products have various morphologies and crystal structures, and control of these variations can be used to generate new functional materials.

When calcium carbonates form under simulated body-environment conditions in the absence of phosphate (PO_4) ions, ACC appears as an initial phase (Brecevic and Nielsen 1989, Gebauer et al. 2010, Mann 2001, Sohnel and Mullen 1982, Weiner et al. 2003). The ACC nucleates by accumulation of calcium carbonate clusters and contains many water molecules in aggregate form, so it has a loose inner structure (Brecevic and Nielsen 1989, Pouget et al. 2009, Pouget et al. 2010, Raiteri and Gale 2010). Because the ACC is in a rather unstable phase and has the highest solubility among the calcium carbonate polymorphs, it rapidly transforms into vaterite via direct structure reconstruction in solution (Brecevic and Nielsen 1989, Pouget et al. 2009, Pouget et al. 2010, Raiteri and Gale 2010).

Vaterite is also in an intermediate and unstable phase (Plummer and Busenberg 1982, Pouget et al. 2009, Pouget et al. 2010, Sunagawa 2005). The higher solubility of vaterite than that of calcite in neutral to weak basic pH solutions results in vaterite dissolution as the calcite nucleates and grows (Rodriguez-Blanco et al. 2010). Phase transformation of

vaterite into calcite proceeds via simple dissolution and growth, in contrast to that of ACC into vaterite (Rodriguez-Blanco et al. 2010). Although calcite is the thermodynamically most stable calcium carbonate under biological conditions, it does not always appear in the hard tissue of non-vertebrates, suggesting that mimicking biomineralization requires that the appearance of intermediate phases be controlled (Mann 2001, Sunagawa 2005, Weiner et al. 2003).

The appearance and phase transformation of each calcium carbonate phase described above occurs in the absence of PO_4. However, the body fluids of non-vertebrates contain PO_4 although the amount is far smaller than that in the body fluids of vertebrates. This PO_4 plays an essential role in the nucleation and growth of calcium carbonates. Previous investigations have shown that the PO_4 extends the lifetime of ACC by stabilizing it, which slows down the formation of crystalline calcium carbonates (Akiva-Tal et al. 2011, Bentov et al. 2010, Sato et al. 2011). However, this stabilization mechanism is still quantitatively unclear.

Under high pH conditions (~10), the presence of PO_4 ions in the solution stabilizes the initially formed vaterite by decreasing the rate of its transformation into calcite (Katsifaras and Spanos 1999). However, there has been little investigation of the effect of PO_4 on the appearance of vaterite under pseudo-physiological (neutral to weak basic pH) conditions.

We investigated the effect of PO_4 on the phase transformation of ACC into vaterite under the pseudo-physiological conditions of non-vertebrates. We derived an advanced concept for cluster-based phase transformation and showed a small amount of PO_4 could be used to easily control the nucleation and growth process of calcium carbonate polymorphs.

2. Experimental

2.1. Preparation of PO_4-containing calcium carbonate solutions

All reagents were purchased from Wako Pure Inc., Japan. We first prepared four mother solutions: 1 M of $CaCl_2$, 2 M of Na_2CO_3, 25 mM of NaCl and KH_2PO_4, and 62.5 mM of tris(hydroxymethyl)aminomethane (Tris). The pH of the Tris solution was adjusted to 8.0 using HCl.

Next, two stock solutions (A and B) were prepared. Solution A was made by adding 0.5 mL of $CaCl_2$ solution and 40 mL of Tris solution to 9 mL of H_2O. Solution B was made by mixing 0.25 mL of Na_2CO_3 with various volumes of NaCl and KH_2PO_4. The volume of KH_2PO_4 in solution B ranged from 0 to 0.25 mL and that of NaCl was the volume needed so that the ionic strength of the solution was 0.055 $(M/L)^2$.

Supersaturated calcium carbonate solutions were prepared by mixing solutions A and B at a volume ratio of 99:1. As they were mixed, they were stirred at 400-600 rpm with a magnetic stirrer. The ionic concentrations in the final solutions were 10 mM of Ca^{2+} and CO_3^{2-}, 0-125 μM of PO_4^{3-}, and 50 mM of Tris. The pH of the final solutions was at 8.2-8.3. The reacting solutions were stirred at 400-600 rpm during each measurement. The solution-containing vessels were sealed using transparent film to avoid a change in concentration due to evaporation. The atmosphere above the solution was not intentionally controlled, but it soon reached equilibrium after measurement was started due to the closed system. All measurements were performed at room temperature (~25°C).

2.2. Measurement of Ca ion concentration and pH as a guide for calcium carbonate

nucleation

The change in the Ca-ion concentration of each solution over time as it was being stirred at 400-600 rpm was measured using a Ca-ion electrode (6583-10C, Horiba Co., Kyoto, Japan) connected to a multi-meter (D-51AC, Horiba Co., Kyoto, Japan). The electrode was soaked in solution A for at least 30 min prior to measurement to stabilize the electrode intensity. Solution B was then added to solution A using a micropipette to start the reaction. The Ca-ion concentration of the mixed solution was measured every 2 s, and the nucleation time of the material was determined using a concentration-time curve (as described in the Results section).

The change in pH of four representative solutions (PO_4 concentrations of 0, 10, 20, and 62.5 μM) over time was measured using a pH electrode (6636-10D, Horiba Co., Kyoto, Japan) connected to a multi-meter (D-51AC, Horiba Co., Kyoto, Japan). The solutions were stirred in the same manner as those in the Ca-ion monitoring experiments.

2.3. Observation of calcium carbonate precipitates using electron microscopies

The calcium carbonate solutions (~60 μL) were sampled at specific intervals to observe the change in precipitate morphology and to identify the types of polymorphs present during phase transformation. The interval was 3 min for the first 6 min and then 20 min for the duration of the experiment.

Two processes were used for the electron microscopy observations. In the first one, 2 mL of 99.5% ethanol or 99.5% acetone was added to the sample solution to immediately stop further reaction. The mixed solution was then centrifuged for 1-2 min. After centrifugation, the precipitates were gathered and washed using ethanol or acetone

144 2 or 3 times and then left to air dry.

145 In the second process, the sample solution was directly centrifuged for 1-2 min, and
146 the precipitates were immediately soaked in ethanol sherbet for 1 min. They were then
147 placed in a vacuum vessel for more than 5 h to be freeze-dried.

148 We observed the precipitates using scanning electron microscopy (SEM) and
149 transmission electron microscopy (TEM) and characterized them using x-ray diffraction
150 (XRD) and selected-area electron diffraction (SAED). No differences were observed in
151 the precipitate morphology or polymorph type regardless of the process used.

152 The treated precipitates were placed on a glass slide for field-emission SEM
153 (FE-SEM; S-4300, Hitachi Co., Tokyo, Japan, Tohoku University; S-4500, Hitachi Co.,
154 Tokyo, Japan, Waseda University) observation after Pt-Pd coating or on an amorphous
155 carbon film or amorphous carbon holey film for TEM (H-8100, Hitachi, Co., Tokyo,
156 Japan, and HF2200, Hitachi, Co., Tokyo, Japan) observation. The films were prepared
157 on conventional Cu grids for TEM. The acceleration voltage and amplitude for the
158 FE-SEM observations were 3-5 kV and 10 μA. The acceleration voltage for the TEM
159 observations was 200 kV. SAED patterns were obtained to characterize the materials.

160 In addition to observing precipitates, we measured the P ion concentration of
161 amorphous calcium carbonate particles using energy dispersive x-ray spectroscopy
162 (EDX) (EDAX GENESIS 5000, AMETEK Inc., USA, combined with a HF2200-type
163 scanning TEM with high-angle annular dark field mode: STEM-HAADF).

164 XRD (X'Pert-MPD, PW3050, Philips Co., Nederland, wavelength = 0.15406 nm)
165 measurements at an acceleration voltage of 50 kV and amplitude of 50 mA using a Cu
166 target were done to characterize the materials. The 2θ step was 0.02^{o}. We varied 2θ
167 from 15^{o} to 80^{o}, and the required time per each step was 0.75 s. Entrance slit size was

5×10 mm. The samples were prepared by sampling 5-10 mL solutions and then using 99.5% ethanol or 99.5% acetone more than ten times to stop further reaction. After the samples were centrifuged, they were washed using 99.5% ethanol or 99.5% acetone 2 or 3 times and then left to air dry.

3. Results

3.1. Change in Ca-ion concentration and pH over time for different PO_4 concentrations in relation to appearance of calcium carbonate polymorphs

We measured the change in the Ca-ion concentration in the solutions over time for the different amounts of PO_4. Figure 1a shows the results for five representative PO_4 concentrations: 0, 3, 10, 20, and 62.5 μM. Except for the 62.5 μM solution, the Ca-ion concentration immediately decreased to 3-5 mM as soon as solution B was added to solution A. It then quickly increased to 6-7 mM. This process was completed within 10 s. The concentration then gradually increased and reached a local equilibrium (seen as a plateau in the figure). The rate of increasing gradually decreased over time. The time required to reach the maximum Ca-ion concentration showed a characteristic relationship with the PO_4 concentration. It took a minimum when the concentration was 3 μM and then increased with the PO_4 concentration.

The Ca-ion concentration decreased after it reached the maximum point and then stabilized at around at 0.3-0.6 mM. The rate of decrease was lower the higher the PO_4 concentration. This decrease was not observed for the solution containing 62.5 μM of PO_4.

We monitored the change in pH in relation to the formation of each polymorph for four representative PO_4 concentrations: zero (only vaterite precipitated as crystalline

192 phase), 10 (vaterite and calcite co-precipitated), 20 (calcite mainly precipitated), and
193 62.5 μM (no precipitation of crystalline phase). The results are shown in Fig. 1d.

194 The precipitates that formed during the plateau interval were observed using SEM
195 and TEM. The sample solutions contained spherical particles ranging in the size from
196 10 to 100 nm (Fig. 1b). The SAED pattern for a particle in Fig. 1c shows a halo without
197 any remarkable Debye rings, indicating that the particles were ACC. The formation of
198 ACC particles was observed for all solutions regardless of the PO_4 concentration.

199 Observation of ACC particles using STEM-HAADF/EDX showed that they
200 contained a trace amount of PO_4. For example, the atomic ratio of Ca/P was ~15 for
201 particles formed in the solution containing 20 μM PO_4. The P ions were
202 inhomogeneously distributed in ACC particles and two-dimensional concentration
203 mapping of the P ions was impossible, probably due to average their low average
204 concentration. The effect of PO_4 on ACC formation will be discussed later.

205 As described in the following sections, crystalline phases (vaterite and calcite)
206 subsequently formed after ACC were observed in the solution. We define the point at
207 which the Ca-ion concentration is maximum as the point at which crystalline calcium
208 carbonates start to grow via phase transformation of ACC. We refer to this
209 crystallization threshold point as t_{cryst}.

210 Fig. 1e shows the relationship between t_{cryst} and the PO_4 concentration. For the
211 solutions containing less than 5 μM PO_4, t_{cryst} decreased with an increase in the PO_4
212 concentration up to 2-3 μM (where t_{cryst} was minimum at ~70 s) and then it increased.
213 The appearance of a minimum point at around 2-3 μM is consistent with the results
214 shown in Fig. 1a. For the solutions containing 5 to 15 μM PO_4, t_{cryst} was very sensitive
215 to the PO_4 concentration. An approximate doubling of the concentration increased t_{cryst}

about 20 times. When the PO_4 concentration exceeded 15 μM, the features observed at 0 to 15 μM were repeated. The t_{cryst} hit a local minimum at 17 μM PO_4 and then exponentially increased when the concentration increased beyond 20 μM.

For the solutions containing more than 24 μM PO_4, the Ca-ion concentration was very stable over the course of the experiment (~2.5 h), the same as for the solution containing 62.5 μM PO_4. The only decrease in the concentration was a rapid one immediately after adding solution B to solution A. This made it impossible to determine t_{cryst} for these solutions.

3.2. Time evolution of calcium carbonate precipitates

The growth and phase transformation of calcium carbonates over time depended on the PO_4 concentration.

3.2.1. Solutions containing less than 5 μM PO_4

Figure 2 shows a time evolution of precipitates in PO_4-free solution. ACC particles 10-100 nm in size formed immediately after solution preparation (see Fig. 1b). There was no other calcium carbonate phase except ACC until reaching t_{cryst}. After t_{cryst}, spherulites with an awkward shape (1-5 μm in length) appeared (Fig. 2a). They were composed of rigid needle-like crystals 0.5-2 μm in length and 10-100 nm in thickness (Figs. 2b and d). These crystals were tightly packed and arranged. They were radially elongated from the center of the spherulites. The spherulites grew over time, and their morphology became spherical by 20 min after solution preparation (Fig. 2c). The needle-like crystals separated from each other during this period, and grain boundaries formed (Fig. 2d). The number of ACC particles was greatly reduced when the spherulites were observed at around t_{cryst}.

The spherulites were observed using SAED to characterize the precipitates at the microscopic level. Three Debye rings, although incomplete, were identified in the outer region of the spherulites. They nearly corresponded to the (114), (300), and (118) diffractions of vaterite (Fig. 2e). The rings were not observed in the inner region of spherulite due to the thickness of the materials (too thick for an electron beam to penetrate) (Fig. 2f).

Figure 3 shows XRD patterns for spherulites measured at 20 and 120 min after solution preparation. Both patterns were essentially the same: they consisted of a broad peak at around 2θ = 20-35^{o} (peak maximum at around 25^{o}), which is characteristic of ACC. The sharp peaks (solid circles) corresponded to vaterite. The observed peak indices were almost consistent with those observed in SAED (Fig. 2e).

The amount of ACC and the intensity of the broad peak at around 2θ = 20-35^{o} suggests that the vaterite spherulites contained an ACC-resembling structure, probably in their central region. Since the phase transformation of ACC into vaterite is typically direct structure reconstruction, the outer growth region of ACC aggregates is more likely to have transformed into vaterite, leaving an amorphous-like structure in the central region.

We concluded that the spherulites were vaterite, and that no other crystalline calcium carbonate polymorphs (calcite or aragonite) formed when the PO_4 concentration was less than 5 μM.

The morphology of the vaterite spherulites (Fig. 2c) did not show any notable change over the course of the experiment (2.5 h).

3.2.2. Solutions containing 5 to 15 μM PO_4

Figure 4 shows the time evolution of precipitates in solution containing 12 μM PO_4. ACC spherical particles 10-100 nm in size formed immediately after solution preparation (Fig. 4a), the same as seen when the PO_4 concentration was less than 5 μM.

Two kinds of precipitates were observed after t_{cryst}: vaterite spherulites and rectangular crystals (0.5-5 μm in size, Fig. 4b), the characteristic morphology of calcite crystals. The surface of the crystals was essentially smooth, and some crystals had coalesced into the vaterite spherulites (Figs. 4b and c).

The amount and size of the calcite crystals increased over time, indicating that transformation of ACC into calcite and subsequent growth proceeded when the solution contained 12 μM PO_4. The vaterite spherulites also grew over time but the growth rate was less than that of calcite (Fig. 4d). The growth rates of these polymorphs were roughly estimated to be ~300 nm/h in calcite and ~200 nm/h in vaterite. Both polymorphs no longer grew after 100 min of solution preparation in FE-SEM observation.

Figure 5 shows XRD patterns for precipitates measured at 20 and 120 min after solution preparation. Peaks corresponding to calcite (solid reverse triangles) and to vaterite (solid circles) were identified. The intensities of the peaks corresponding to calcite increased over time, indicating that the volume of calcite relative to that of vaterite gradually increased over time. This was also observed when we compared the volume of both polymorphs in relation to the concentration of PO_4 at a particular time. Increasing the PO_4 concentration resulted in an increase in the calcite ratio. However, the absolute volume of vaterite was far larger than that of calcite during the experimental procedure (~2.5 h) when the PO_4 concentration was less than 15 μM. The volume ratio between vaterite and calcite in solution containing 15 μM PO_4 was

288 estimated at around t_{cryst} to be ~5:1.

289

290 3.2.3. Solutions containing more than 15 μM PO_4

291 Figure 6 shows the time evolution of precipitates in solution containing 20 μM PO_4.
292 Immediately after solution preparation, ACC particles 10-100 nm in size appeared, as
293 they did when the PO_4 concentration was less than 15 μM (Fig. 6a). Fig. 6b shows the
294 SAED pattern for vaterite spherulites. After t_{cryst}, vaterite spherulites and rectangular
295 calcite crystals were observed, as they were in the solutions containing 5 to 15 μM PO_4.
296 Fig. 6d shows the SAED pattern for vaterite spherulites. Four Debye rings
297 corresponding to (112), (114), (300), and (118) diffractions were identified. Each ring
298 contained many Laue spots, indicating that the crystallinity of the outer region was high.
299 Fig. 6e shows that vaterite and calcite coexisted. Their relative volume was the
300 reverse of that for the 5-15 μM PO_4 condition. There was a small number of vaterite
301 spherulites (1-5 μm in diameter) and a large number of calcite crystals (0.5-5 μm in size).
302 The ratio between these polymorphs was ~1:3, estimated using the solutions at around
303 t_{cryst} (40 min after preparation). Vaterite and calcite continued to coexist at a constant
304 volume ratio up to 80 min.
305 A characteristic change in the vaterite morphology was observed at around 80 min
306 after solution preparation. Figs. 6f and g show a vaterite spherulite observed at 100 min.
307 The spherulite had holes in its surface and a hollow structure. TEM observation showed
308 that an electron beam was able to penetrate the center of the spherulites (Fig. 6g), as
309 expected from Fig. 6c. This morphology suggests that the spherulites dissolved first in
310 their center region. The vaterite eventually disappeared: many vaterite casts remained
311 on the surface of the calcite crystals (Fig. 6h).

XRD measurement showed that the ratio of calcite to vaterite increased over time (Fig. 7). XRD patterns measured 120 min after solution preparation showed that the peaks corresponding to vaterite had disappeared and that only those corresponding to calcite were evident. SEM and TEM observations and XRD measurements indicated that the dissolution of vaterite and the growth of calcite occurred over time. Phase transformation of vaterite into calcite proceeded via a simple dissolution and growth mechanism. Evidence of direct structure-reconstruction-type transformation between these polymorphs was not observed.

When the PO_4 concentration exceeded 25 μM, precipitation of calcite was not observed. ACC particles that appeared immediately after solution preparation survived the experimental procedure (2.5 h). Time evolution of polymorph precipitation and the polymorph morphology for each PO_4 concentration are summarized in Table 1.

4. Discussion

Analysis of the relationships between t_{cryst}, polymorph type and PO_4 concentration showed that PO_4 inhibited vaterite formation because t_{cryst} increased exponentially with the PO_4 concentration for concentrations ranging from 5 to 15 μM, where vaterite was observed as the major precipitates. The change in t_{cryst} when the PO_4 concentration was less than 5 μM is discussed below.

Previous investigations of the formation of calcium carbonate polymorphs in the presence of PO_4 demonstrated that the PO_4 extends the lifetime of ACC by stabilizing it. However, our investigation demonstrated that the PO_4 inhibits vaterite formation and does not affect the nucleation and growth of ACC. ACC formed immediately after solution preparation. The change in the Ca-ion concentration due to the formation of

ACC in this initial stage was independent of the PO_4 concentration, as seen in Fig. 1a.

The change in the formation of calcium carbonate polymorphs with a change in the PO_4 concentration suggests that PO_4 affects the phase transformation (from ACC) and growth of polymorphs kinetically and that it does not control the stability of each phase. The solubility of each polymorph, at least the solubility ordering, was not affected by the PO_4 concentration because the polymorph appearance order obeyed the Ostwald's step law, the same as in the absence of impurities.

So how does PO_4 control the formation of polymorphs, especially that of vaterite, at the microscopic level? We assume that the PO_4 inhibition mechanism is related to the growth unit of calcium carbonates, i.e., the species of molecular clusters. Gebauer et al. proposed a prenucleation cluster model for crystalline calcium carbonate growth. By using extended x-ray adsorption fine structure and ultracentrifuge techniques, they showed that clusters 2-4 nm in diameter form even in undersaturated solutions with respect to calcite and vaterite and that ACC contains these clusters as the essential growth unit (Gebauer et al. 2008). The clusters have particular structures corresponding to those of calcium carbonate polymorphs; therefore, the ACC particles are assumed to have several kinds of local structure in this model, such as ACC1 and ACC2. When ACC transforms into calcite or vaterite, as in this study, particular ACC particles have a rearranged inner structure corresponding to the final crystalline phases.

According to this model, there are two possible mechanisms for PO_4 inhibiting vaterite formation. One is that the PO_4 inhibits the structure-reconstruction of ACC into vaterite. The other is that PO_4 simply hinders the formation (growth) of vaterite clusters in the same manner as impurities do. Regardless of the mechanisms the behavior of PO_4 should be monotonic; that is, its effectiveness should increase with its concentration.

However, the change in t_{cryst} when the concentration was less than 5 μM is inconsistent with this assumption. The appearance of a minimum t_{cryst} at a PO_4 concentration of around 2-3 μM requires a modification of the model to explain the effect of PO_4 on vaterite formation.

We assume that there are several candidate clusters corresponding to the vaterite structure; i.e., there are many isomers. Except for the particular-structure clusters that form the vaterite crystals, many minor clusters would be produced and contained in the initial ACC. The stability of these minor clusters would be controlled by the PO_4 in solution. The inhomogeneous distribution of P ions in the ACC particles observed using STEM-HAADF indicates that P ions are in the cluster voids and do not substitute for CO_3 clusters, which is necessary to control the stability of each cluster when ACC forms.

The idea that molecular clusters can take many different structures, all corresponding to the local energy minimum form, was established by Treboux et al. and Kanzaki et al. using *ab initio* calculations for calcium phosphate clusters having a $Ca_9(PO_4)_6$ chemical composition, the essential unit of amorphous calcium phosphate and hydroxyapatite (Treboux et al. 2000, Kanzaki et al. 2001). Yan and Scott also referred to the multi-structures in $Ca_9(PO_4)_6$ clusters (Yan and Scott 2003).

Our suggestion that vaterite clusters also have several isomers is therefore realistic. The PO_4 would dissociate these minor clusters (or hinder their formation), which would increase the concentration of calcium and carbonate ions in solution. A higher concentration of calcium and carbonates ions would inevitably change the chemical equilibrium between ions and clusters corresponding to those forming the vaterite crystal-structure, and the concentration of these clusters would be increased. This would

naturally lead to a decrease in the t_{cryst} of vaterite. We assume that competition between acceleration caused by dissociating isomers and inhibition of the transformation of the ACC structures into vaterite ones occurred in the solution and that the minimum t_{cryst} appeared.

The PO_4 similarly affected the calcite formation when its concentration ranged from 15 to 24 μM, the range in which calcite was the major precipitate. The minimum t_{cryst} appeared at around 17 μM, and t_{cryst} increased exponentially when the concentration exceeded 20 μM. This feature is essentially the same as that seen in vaterite formation, meaning that there are several isomers in calcite clusters. The difference between calcite formation and vaterite formation is the decreasing rate at minimum t_{cryst}. The minimum t_{cryst} observed in vaterite formation was approximately 40% that for 0 μM PO_4. In contrast, the minimum t_{cryst} observed in calcite formation was approximately 20% that for 15 μM PO_4. This suggests that there is less variety of isomers in calcite clusters as compared to that in vaterite clusters or that PO_4 is less effective in dissociating the isomers in calcite clusters.

5. Conclusion

Our experiments showed that a small amount of PO_4 in the Ca-CO_3-PO_4 system did not extend the lifetime of amorphous calcium carbonate but did inhibit vaterite formation. The inhibition mechanism is not analyzed if we assume that the clusters forming the vaterite crystal structure have a unique form when they are produced in solution and they are composed of ACC. The idea that vaterite clusters have several isomers could explain the experimental results. This investigation showed that the

appearance and stability of calcium carbonate polymorphs is easily controlled by adjusting the PO_4 concentration.

Acknowledgments: We thank Dr. T. Yamada for helping with the XRD measurements, Prof. T. Ito and Mr. R. Kuwano for helping with the FE-SEM observations, and Dr. Y. Sogo for helping with the Ca-ion concentration measurements. We also thank Dr. H. Miura for his useful suggestions. This work was supported in part by the Tohoku University Global COE Program for “Global Education and Research Center for Earth and Planetary Dynamics,” by the Center for Interdisciplinary Research (CIR), Tohoku University, and by the Material Characterization Central Laboratory, Waseda University.

421

422 **References**

423 Addadi, L., Raz, S., Weiner, S. (2003) Taking Advantage of Disorder: Amorphous
424 Calcium Carbonate and its Roles in Biomineralization, Advanced Materials, 15,
425 959-970.
426 Akiva-Tal, A., Kababya, S., Balazs, Y.S., Glazer, L., Berman, A., Sagi, A., Schmidt, A.
427 (2011) In situ molecular NMR picture of bioavailable calcium stabilized as amorphous
428 $CaCO_3$ biomineral in crayfish gastroliths, Proceeding of the National Academy of
429 Science of USA, 36, 14763-14768.
430 Bentov, S., Weil, S., Glazer, L., Sagi, A., Berman, A. (2010) Stabilization of amorphous
431 calcium carbonate by phosphate rich organic matrix proteins and by single
432 phosphoamino acids Journal of Structural Biology, 171, 207-215.
433 Brecevic, L. and Nielsen, A.E. (1989) Solubility of Amorphous Calcium Carbonate,
434 Journal of Crystal Growth, 98, 504-510.
435 Gebauer, D., Gunawidjaja, P.N., PeterKo, J.Y., Bacsik, Z., Aziz, B., Liu, L., Hu, Y.,
436 Bergstrom, L., Tai, C.W., Sham, T.K., Eden, M., Hedin, N. (2010) Proto-Calcite and
437 Proto-Vaterite in Amorphous Calcium Carbonates, Angewande Chemie International
438 Edition, 49, 8889-8891.
439 Gebauer, D., V lkel, A., Colfen, H. (2008) Stable Prenucleation Calcium Carbonate
440 Clusters, Science, 322, 1819-1822.
441 Katsifaras, A. and Spanos, N. (1999) Effect of inorganic phosphate ions on the
442 spontaneous precipitation of vaterite and on the transformation of vaterite to calcite,
443 Journal of Crystal Growth, 204, 183-190.
444 Kanzaki, N., Treboux, G., Onuma, K., Tsutsumi, S., Ito, A. (2001) Calcium Phosphate

Clusters, Biomaterials, 22, 2921-2929.

Kraji, D. and Brecevic, L. (1995) Dissolution kinetics and solubility of calcium carbonate monohydrate, Colloid and Surface A: Physicochemical and Engineering Aspects, 96, 287-293.

Mann, S. (2001) *Biomineralization Principles and Concepts in Bioinorganic Materials Chemistry*, Oxford University Press, UK.

Pouget, E.M., Bomans, P.H.H., Dey, A., Frederik, P.M., de With, G., Sommerdijk, N.A.J.M. (2010) The development of morphology and structure in hexagonal vaterite, Journal of American Chemical Society, 132, 11560-11565.

Pouget, E.M., Bomans, P.H.H., Goos, J.A.C.M., Frederik, P.M., de With, G., Sommerdijk, N.A.J.M. (2009) The Initial Stages of Template-Controlled CaCO3 Formation Revealed by Cryo-TEM, Science, 323, 1455-1458.

Plummer, L.N. and Busenberg, E. (1982) The solubilities of calcite, aragonite and vaterite in CO_2-H_2O solutions between 0 and 90^{o}C, and an evaluation of the aqueous model for the system $CaCO_3$-CO_2-H_2O, Geochimica et. Cosmochimica Acta, 46, 1011-1040.

Raiteri, P. and Gale, J.D. (2010) Water Is the Key to Nonclassical Nucleation of Amorphous Calcium Carbonate, Journal of American Chemical Society, 132, 17623-17634.

Rodriguez-Blanco, J.D., Shaw, S., Benning, L.G. (2010) The kinetics and mechanisms of amorphous calcium carbonate (ACC) crystallization to calcite, via vaterite, Nanoscale, 3, 265-271.

Sato, A., Nagasaka, S., Furihata, K., Nagata, S., Arai, I., Saruwatari, K., Kogure, T., Sakuda, S., Nagasawa, H. (2011) Glycolytic intermediates induce amorphous calcium

carbonate formation in crustaceans, Nature Chemical Biology, 7, 197-199.

Sohnel, O. and Mullin, J.W. (1982) Precipitation of Calcium Carbonate, J. Crystal Growth, 60, 239-250.

Sunagawa, I. (2005) *Crystals Growth, Morphology and Perfection*, Cambridge University Press, UK.

Treboux, G., Layrolle, P., Kanzaki, N., Onuma, K., Ito, A. (2000) Symmetry of Posner's Cluster, Journal of American Chemical Society, 122, 8323-8324.

Weiner, S. and Dove, P.M. (2003) In P. M. Dove, J. J. DeYoreo and S. Weiner, Eds., *Biomineralization*, *Reviews in Mineralogy and Geochemistry*; Dove, P.M., DeYoreo, J.J., Weiner, S., Eds.; The Mineralogical Society of America: Washington, DC, Vol. 54, p. 249.

Yin, X. and Stott, M.J. (2003) Biological calcium phosphates and Posner's cluster, Journal of Chemical Physics, 118, 3717-3723.

493 **Figure and Table Captions**

494 Table 1: Observed calcium carbonate polymorphs and time evolution of polymorph
495 morphology for each PO_4 concentration.

496

497 Figure 1: Change in Ca-ion concentration over time as index of calcium carbonate
498 formation. (a) Ca-ion concentration rapidly dropped immediately after mixing but
499 quickly recovered at initial stage (left graph). It then decreased over time (right graph)
500 and stabilized at around 0.3-0.6 mM, except for 62.5 μM of PO_4. (b) TEM photograph
501 of spherical particles that formed immediately after preparation in PO_4-free solution. (c)
502 Change in pH over time as index of calcium carbonate formation. It rapidly increased
503 after mixing and stabilized at around 8.1-8.4 depending on PO_4 concentration. (d)
504 SAED pattern corresponding to (b). Particles were ACC as identified by halo region
505 around core and faint broad ring around halo region. (e) Relationship between
506 crystallization threshold point t_{cryst} and PO_4 concentration: t_{cryst} was minimum at 2-3 μM
507 of PO_4 (left graph); it then increased exponentially with PO_4 concentration in the 5 to 15
508 μM range. Local minimum in t_{cryst} was again observed at 17 μM, and then t_{cryst} increased
509 exponentially above 20 μM (right graph).

510

511 Figure 2: Time evolution of precipitates in PO_4-free solution. (a) SEM photograph of
512 awkward-shape vaterite spherulite observed 10 min after sample preparation. (b)
513 Needle-like crystal in vaterite spherulite observed 20 min after preparation. (c) SEM
514 photograph of vaterite spherulites (sphere shape) observed 20 min after preparation.
515 High magnification image of round vaterite spherulite. (d) SEM photograph of piece of
516 spherulite. Arrows show grain boundaries. (e) SAED pattern corresponding to (b)

showing (114), (300), and (118) diffractions of vaterite crystal. (f) TEM photograph of vaterite spherulite observed 120 min after preparation. Center structure was not observed due to thickness.

Figure 3: XRD pattern of precipitates in PO_4-free solution measured at 20 and 120 min after preparation. Peaks corresponding to ACC and vaterite (solid circles) are evident. Tables show 2θ, d-spacing, and relative intensity corresponding to identified (*hkl*) indices of precipitated phase at 20 and 120 min after solution preparation. *V* indicated vaterite.

Figure 4: Time evolution of precipitates in solution containing 12 μM. (a) TEM photograph of ACC spherical particles that formed immediately after preparation. SAED pattern (inset at upper right) showed halo region around core and faint broad ring around halo region. (b) SEM photograph of rectangular calcite crystal and vaterite spherulite 20 min after preparation. Calcite crystal had coalesced into vaterite spherulite. (c) SEM photograph of calcite crystal 20 min after preparation. Surface was essentially smooth indicating that PO_4 did not have adsorbed on the surface as an inhibitor. (d) SEM photograph showing coexistence of vaterite spherulites with calcite crystals 120 min after preparation. Both vaterite and calcite had continued to grow.

Figure 5: XRD patterns for precipitates in solution containing 12 μM PO_4 at 20 and 120 min after preparation. Peaks corresponding to ACC, vaterite (solid circles) and calcite (solid reverse triangles) are evident. The calcite/vaterite ratio increased over time. Tables show 2θ, d-spacing, and relative intensity corresponding to identified (*hkl*)

541 indices of precipitated phase at 20 and 120 min after solution preparation. *V* and C
542 indicate vaterite and calcite, respectively.
543
544 Figure 6: Time evolution of precipitates in solution containing 20 μM PO_4. (a) TEM
545 photograph of ACC spherical particles immediately after preparation. (b) SAED pattern
546 corresponding to (a). (c) TEM photograph of vaterite spherulites observed 40 min after
547 preparation. (d) SAED pattern corresponding to (c). Diffraction indexes coincided with
548 those of vaterite. Vaterite center was too thick for electron beam to penetrate. (e) SEM
549 photograph of calcite rectangular crystals coexisting with vaterite spherulites 40 min
550 after preparation. (f) SEM photograph of calcite rectangular crystals coexisting with
551 hollow vaterite spherulites 100 min after preparation. Core of vaterite spherulites had
552 vanished so that only outer shell remained. (g) TEM photograph of vaterite spherulites.
553 Note that electron beam was able to penetrate center region of spherulites. (h) SEM
554 photograph of calcite crystal 120 min after preparation. Cast where vaterite dissolved
555 and disappeared is evident.
556
557 Figure 7: XRD patterns for precipitates in solution containing 20 μM PO_4 at 40 and 120
558 min after preparation. Peaks corresponding to ACC, vaterite (solid circle) and calcite
559 (solid reverse triangle) are evident for 40 min while only the peaks corresponding to
560 calcite are evident for 140 min. Tables show 2θ, d-spacing, and relative intensity
561 corresponding to identified (*hkl*) indices of precipitated phase at 40 and 120 min after
562 solution preparation. *V* and C indicate vaterite and calcite, respectively.
563

564

565

pH	pH = 8.0-8.4, room temperature and pressure			
Ionic strength	Ionic strength = 0.137 $[M/L]^2$, Ca = 10 mM/L, CO_3 = 10 mM/L, PO_4 = 0-125 μM/L			
Mixing method	Stirring at 400-600 rpm using magnetic stirrer			
Drying method	Washing precipitate in ethanol or acetone to remove water, and eventually dried			
	PO_4 free	PO_4 10 μM	PO_4 20 μM	PO_4 62.5 μM
0 min	ACC spherical particles	ACC spherical particles	ACC spherical particles	ACC spherical particles
10 min	Vaterite spherulite, ACC spherical particles	ACC spherical particles	ACC spherical particles	ACC spherical particles
20 min	Vaterite spherulite, ACC spherical particles	Vaterite spherulite, Calcite rectangular crystal	ACC spherical particles	ACC spherical particles
40 min	Vaterite spherulite, ACC spherical particles	Vaterite spherulite, Calcite rectangular crystal	Vaterite spherulite, Calcite rectangular crystal	ACC spherical particles
60 min	Vaterite spherulite	Vaterite spherulite, Calcite rectangular crystal	Vaterite spherulite, Calcite rectangular crystal	ACC spherical particles
100 min	Vaterite spherulite	Vaterite spherulite, Calcite rectangular crystal	Vaterite halo like structure, Calcite rectangular crystal	ACC spherical particles
120 min	Vaterite spherulite	Vaterite spherulite, Calcite rectangular crystal	Calcite rectangular crystal	ACC spherical particles

566 Table 1

567

568

569

570

571

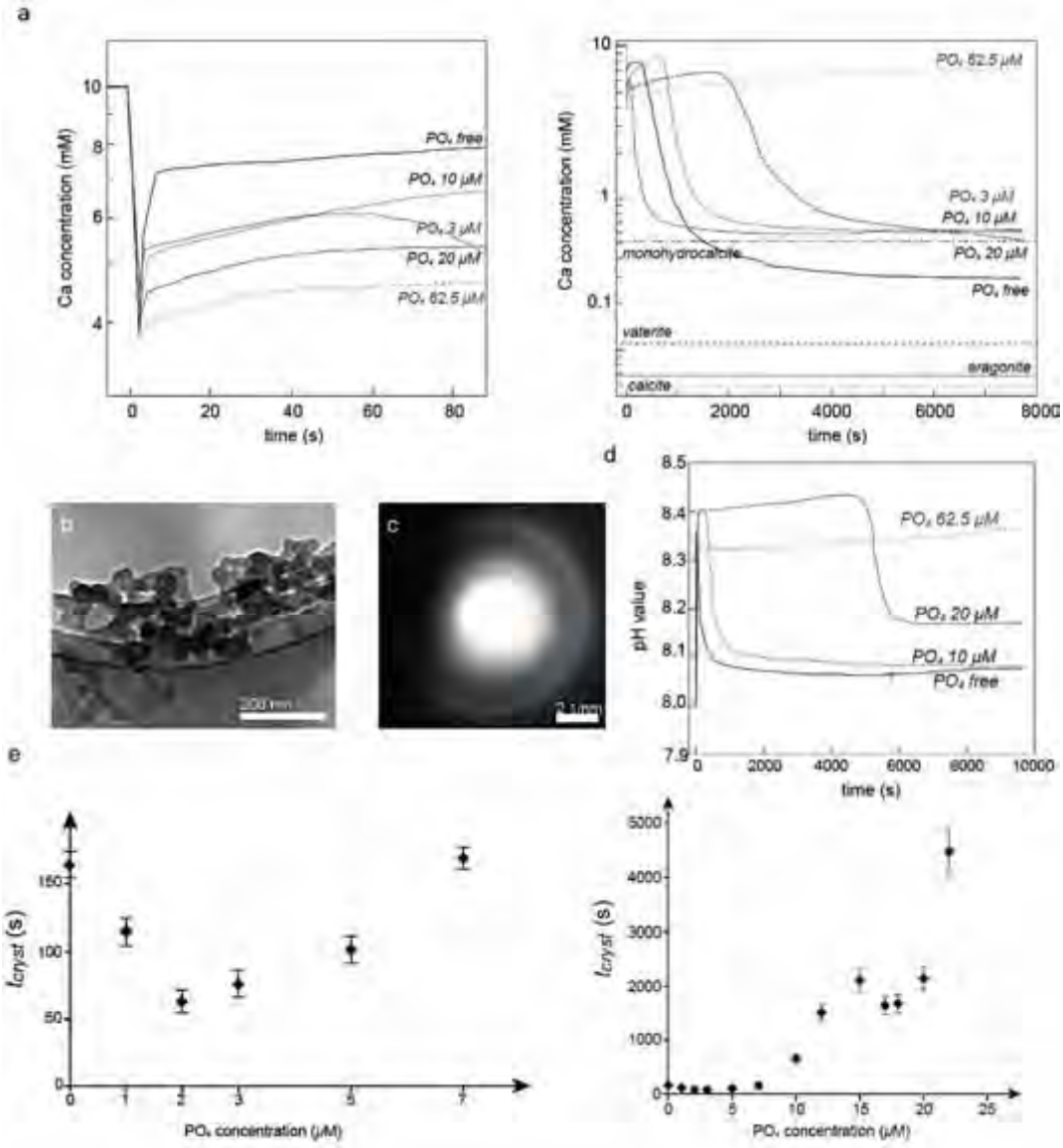

Figure 1

572

573

574

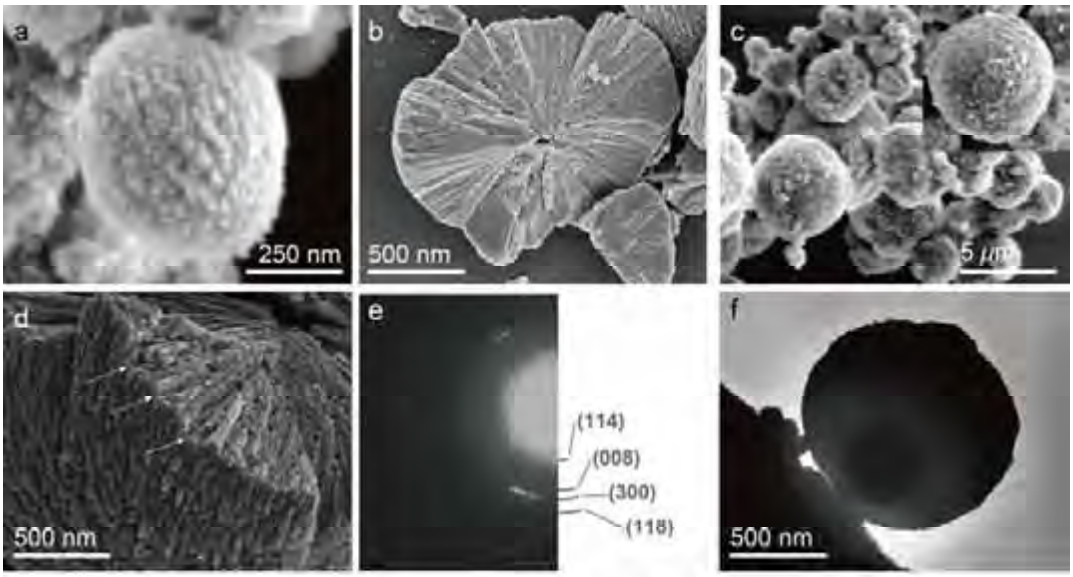

Figure 2

590

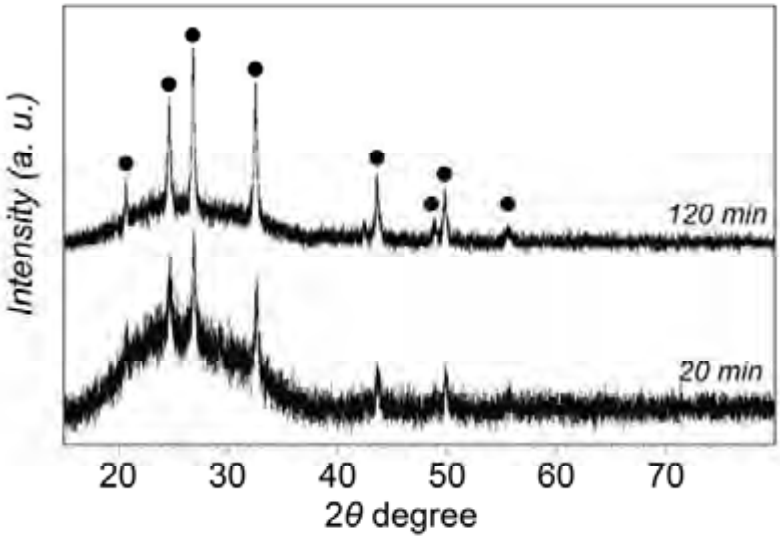

20 min			
2 θ	d spacing	intensity	phase
20.74	4.28	44.3	*V(004)*
24.70	3.62	80.9	*V(110)*
26.88	3.34	100.0	*V(112)*
32.62	2.76	70.3	*V(114)*
42.50	2.14	3.6	*V(008)*
43.68	1.86	23.0	*V(300)*
49.82	1.82	18.0	*V(304)*
55.66	1.66	3.1	*V(224)*

120 min			
2 θ	d spacing	intensity	phase
20.68	4.30	28.7	*V(004)*
24.62	3.60	74.5	*V(110)*
26.80	3.32	100.0	*V(112)*
32.50	2.74	78.9	*V(114)*
42.10	2.12	8.2	*V(008)*
43.90	1.86	32.0	*V(300)*
49.78	1.82	26.2	*V(304)*
55.52	1.66	6.0	*V(224)*

Figure 3

591

592

593

594

595

596

597

598

599

600

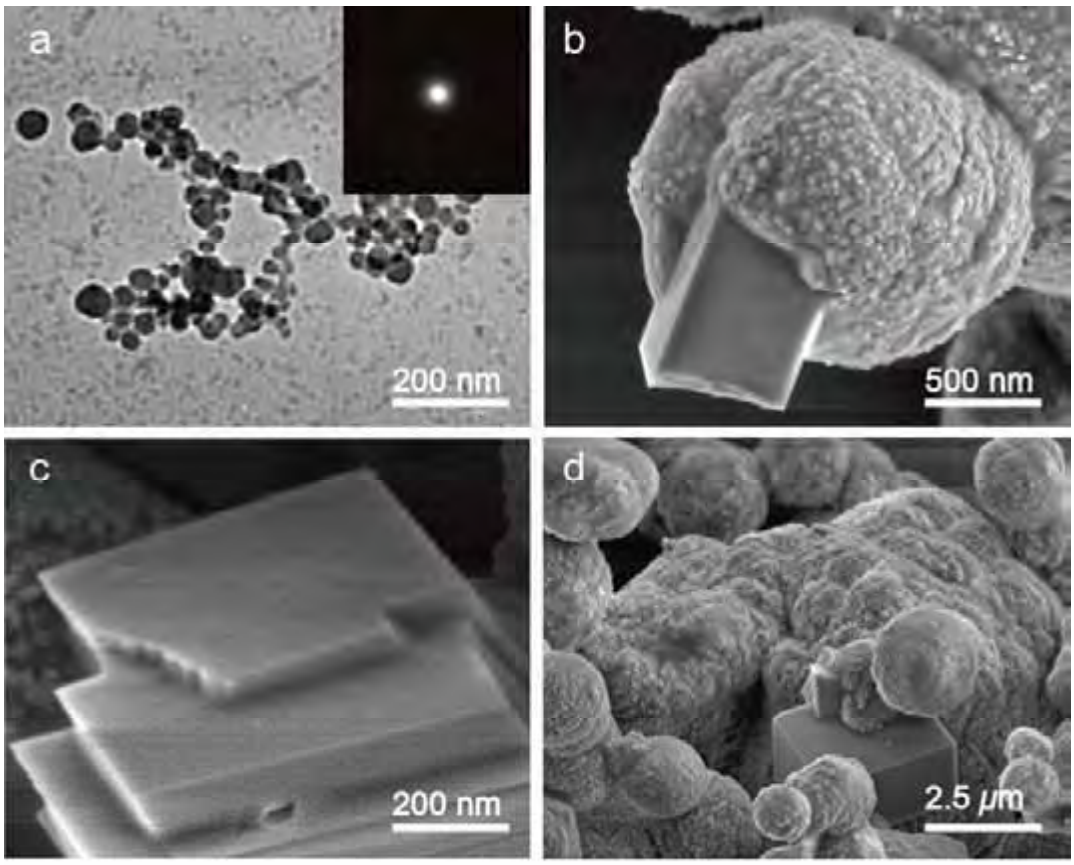

Figure 4

601

602

603

604

605

606

607

608

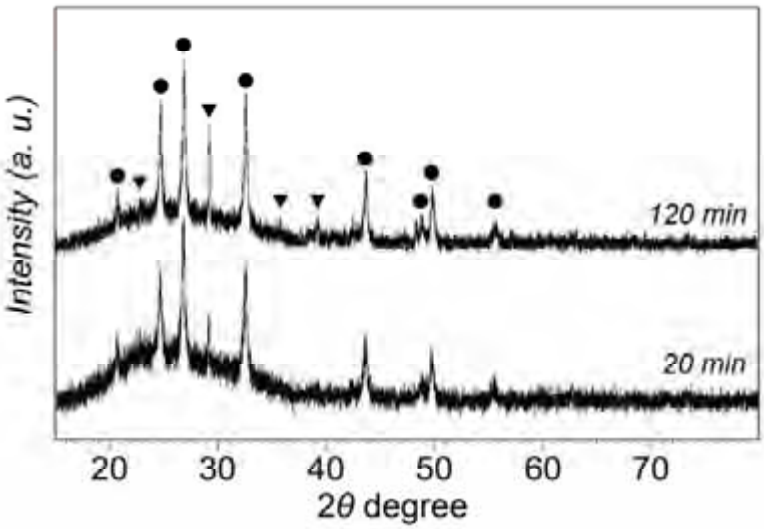

20 min			
2 θ	d spacing	intensity	phase
20.64	4.32	38.3	*V(004)*
24.60	3.62	76.6	*V(110)*
26.76	3.32	100	*V(112)*
29.10	3.06	44.9	**C(104)**
32.50	2.76	74.5	*V(114)*
39.14	2.30	5.9	**C(113)**
42.88	2.12	5.9	**C(202)**
43.62	2.08	29.7	*V(300)*
48.80	1.88	9.58	**C(116)**
49.74	1.84	25.2	*V(304)*
55.58	1.64	6.3	*V(224)*
69.24	1.36	4.7	*V(228)*

120 min			
2 θ	d spacing	intensity	phase
20.78	4.28	18.8	*V(004)*
22.88	3.88	24.0	**C(012)**
24.76	3.58	79.2	*V(110)*
26.90	3.30	100.0	**C(104)**
29.22	3.06	59.4	**C(104)**
32.64	2.74	77.1	*V(114)*
35.92	2.50	6.3	**C(110)**
39.24	2.30	16.7	**C(113)**
42.52	2.12	8.3	**C(018)**
43.72	2.06	38.5	*V(300)*
49.90	1.82	22.9	*V(304)*
55.60	1.64	7.9	*V(224)*

609 Figure 5

610

611

612

613

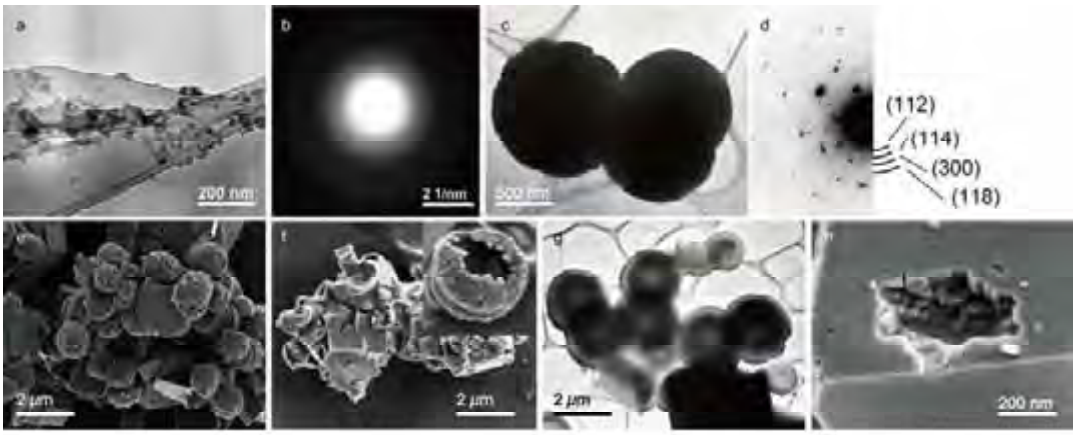

Figure 6

632

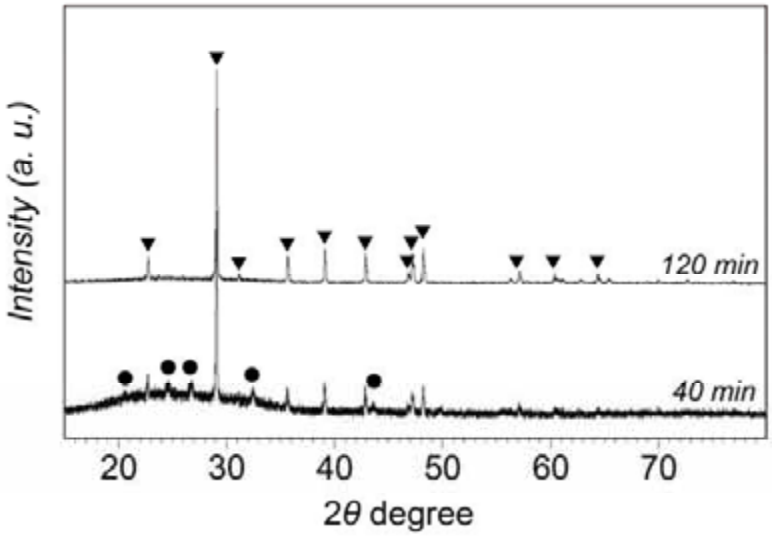

40 min			
2 θ	d spacing	intensity	phase
20.64	4.30	9.1	*V(004)*
22.74	3.92	18.2	**C(012)**
24.58	3.62	13.6	*V(110)*
26.74	3.32	15.1	*V(112)*
29.06	3.08	100.0	**C(104)**
32.48	2.76	11.0	*V(114)*
35.62	2.52	11.7	**C(110)**
39.10	2.32	14.5	**C(113)**
42.82	2.12	13.2	**C(202)**
47.18	1.92	9.8	**C(018)**
48.20	1.88	10.5	**C(116)**
57.08	1.60	4.2	**C(122)**
64.34	1.44	1.7	**C(300)**

120min			
2 θ	d spacing	intensity	phase
22.76	3.92	11.1	**C(012)**
29.10	3.06	100.0	**C(104)**
35.66	2.52	11.5	**C(110)**
39.12	2.30	15.4	**C(113)**
42.86	2.10	12.6	**C(202)**
47.20	1.92	13.4	**C(018)**
48.20	1.88	15.3	**C(116)**
57.12	1.60	5.7	**C(122)**
60.40	1.52	3.9	**C(214)**
64.38	1.44	4.0	**C(300)**

Figure 7

633

634

635

636